Desalination and Water Treatment
www.deswater.com

doi: 10.5004/dwt.2017.0414

58 (2017) 144–153
January

Adsorption of Cr (VI) and Cd (II) on chitosan grafted polyaniline-OMMT nanocomposite: isotherms, kinetics and thermodynamics studies

Rais Ahmad[a], Imran Hasan[a], Alok Mittal[b,*]

[a]*Environmental Research Laboratory, Department of Applied Chemistry, Aligarh Muslim University, Aligarh, 202002, India, Tel. +91- 0571-2700920-23 Ext-3000; Fax: +91- 0571- 2400528; email: rais45@rediffmail.com (R. Ahmad), imranhasan98@gmail.com (I. Hasan)*
[b]*Department of Chemistry, Maulana Azad National Institute of Technology, Bhopal, 462003, India, Tel. 0091-9425025427; Fax: 0091-755-2670562; email: aljymittal@yahoo.co.in*

Received 13 April 2016; Accepted 8 June 2016

ABSTRACT

A novel nanocomposite adsorbent chitosan grafted polyaniline-OMMT (CPOM) was synthesized by oxidative free radical polymerization of aniline in presence of montmorillonite and chitosan. The material was well characterized by FTIR, XRD, TGA, SEM and TEM and engaged for the removal of Cr (VI) and Cd (II) from aqueous solutions. Various parameters such as adsorbent dose, solution pH, metal ion concentration and temperature were studies to find the optimum conditions for adsorption reaction. The equilibrium data were applied to study the Langmuir, Freundlich, Flory-Huggins and Temkin models. On the basis of value of correlation coefficient, the applicability of Langmuir isotherm model was confirmed and maximum monolayer adsorption capacity was found to be 90.90 mg g^{-1} for Cr (VI) and 54.64 mg g^{-1} for Cd (II). The adsorption kinetics data were found to be best followed by pseudo-second-order reaction and the adsorption mechanism was well described by chemisorption. Thermodynamic studies showed that the adsorption process was endothermic and feasible. The results show that the material exhibit a high removal efficiency towards Cr (VI) and Cd (II).

Keywords: Biopolymer; PANI; Graft copolymerization; Flory-Huggins; Montmorillonite; Endothermic

1. Introduction

Increase in industrial and human activities has intensified environmental pollution and the deterioration of water systems with the accumulation of many pollutants, especially heavy metals [1,2]. Among the toxic heavy metals, Cr (VI) and Cd (II) ions have been found to be most toxic heavy metals and are a serious threat to humans as well as marine life even at low concentrations as they can bio accumulate through the food chain [3–5]. Humans can be affected by serious problems, such as dermatitis, allergy, lung and nervous system problems due to Cr (VI) and on the other hand Cd (II) is primarily toxic to kidney and bones [6–8].

Various conventional methods have been developed for the removal of heavy metals from wastewater including precipitation, reduction, membrane filtration, ion exchange, reverse osmosis, and adsorption [9–11]. Of these methods, adsorption has been found to be very efficient for the removal of chromium from contaminated groundwater due to its low initial cost and ease of operation [12,13].

Recently biopolymer grafted synthetic polymer base nanocomposites have gained much attention as adsorbent in the field of wastewater treatment due to combine properties of both biopolymer and synthetic polymer. Chitosan (CTS) is a biopolymer produced by partial deacetylation of naturally occurring biopolymer chitin [14]. Chitosan has been proved as an effective adsorbent due to a number of amino groups that are responsible for the high adsorption property of chitosan [15,16].

* Corresponding author.

Due to large amount of amine and imine functional groups, PANI has strong affinity with metal ions and can remove heavy metal contaminants from aqueous solutions effectively [17,18]. To extend its efficiency for the removal of heavy metals, PANI was grafted with a biopolymer chitosan. The stability of polymer matrix can be enhance by addition of fillers such as natural clays, metal oxide nanoparticles etc. [19]. The naturally occurring sodium montmorillonite (MMT) clay is most commonly used as filler for polymer nanocomposites [20]. MMT has ability to exchange ions to make it suitable for using it as filler in hydrophobic polymers and to prevent its agglomeration in polymer matrix [21].

In this study, CTS grafted PANI-OMMT nanocomposite was synthesized by oxidative free radical graft copolymerization of aniline in presence of montmorillonite and chitosan was further utilized as an adsorbent for removal of Cr (VI) and Cd (II) form aqueous solutions. The adsorption parameters prove that the nanocomposite show a very high adsorption capacity towards Cr (VI) and Cd (II).

2. Materials and methods

2.1. Materials

Sodium montmorillonite, chitosan, cetyltrimethylammonium bromide (CTAB) and ammonium persuphate (APS) were purchased from Sigma-Aldrich India and used as received. Aniline monomer was purchased from Merck, India, and was distilled before use. Potassium dichromate ($K_2Cr_2O_7$) and cadmium nitrate ($Cd(NO_3)_2$) were purchased from Merck, India. 1000 mg L^{-1} stock solutions of corresponding metal ion was prepared by dissolving appropriate amount of metal salts in double distilled water.

2.2. Synthesis of organo-MMT (OMMT)

Synthesis was done by already reported method [22], by using ion exchange process and the detailed method as follows: 5.0 g of montmorillonite was taken in a round bottom flask with 200 mL of double distilled water and vigorously stirred for 1 h at 80°C. Now to the above suspension 100 mL of 0.1 M solution of CTAB was added and the mixture again left on stirring for 2 h. Now the OMMT was filtered and washed to remove extra CTAB and dried at 60°C in a vacuum oven for 2 h.

2.3. Synthesis of chitosan-gft-polyaniline/OMMT nanocomposite

The material chitosan-gft-polyaniline/OMMT (CPOM) was synthesized by oxidative free radical polymerization of Aniline in presence of chitosan [23]. The detailed procedure is as follows: 1 g of chitosan was dissolved in 100 mL of 0.1 M HCl solution in a round bottom flask. Now in another flask 1 g of OMMT was taken in a 100 mL of double distilled water and stirred for 1 h to get well dispersed and this suspension was added to the above chitosan solution and again stirred for 1 h. Now 10 mL of distilled aniline in 150 mL of 0.1 M HCl solution was added to the above mixture at 0°C–5°C temperature followed by addition of APS solution. The reaction was allowed to stand for 12 h on magnetic stirrer and a green coloured precipitate was formed which was filtered and washed by 0.1 M HCl solution to remove unused aniline monomer and later on with double distilled water and was dried at 60°C for 4 h in oven.

2.4. Instrumentation

The FTIR spectra of the adsorbent materials were recorded with a Perkin Elmer 1800 model IR spectrophotometer operating at frequency range from 400 to 4,000 cm^{-1} using KBr pallets. X-Ray diffraction (XRD) patterns of the samples were obtained using Siemens D 5005 X-Ray unit Cu Kα (λ = 1:5406A°) radiation, generated at a voltage of 40 kV and a current of 40 mA was used as the X-ray source. Scanning electron microscopy and Electron diffraction scattering (SEM/EDS) analysis were done using GSM 6510LV Scanning electron microscope. The particle size and structure of the synthesized nanocomposite were observed by using JEM 2100 transmission electron microscope (TEM). The thermal stability was determined by derivative thermal analysis (DTG, Perkin Elmer Pyris 6) and DTA (Perkin Elmer model, STA 6000). The thermograms were recorded for 20 mg of powder sample at a heating rate of 10°C min^{-1} in the temperature range of 30°C–800°C under nitrogen atmosphere.

The concentration of metal ions in the solution was measured by Atomic Absorption Spectrophotometer (AAS) model GBC-902. Elico Li 120 pH meter was used to adjust the pH of the solutions.

2.5. Adsorption experiments

The adsorption experiments were carried out using batch equilibrium technique in aqueous solutions at a pH value of 2 for Cr (VI) and 5 for Cd (II) at 30°C–50°C. 0.05 g of adsorbents was added to 20 mL of 40 mg L^{-1} metal ion solution and shaken in a thermostatic water-bath shaker operated at 120 rpm. After equilibrium was reached, adsorbent was removed and the supernatant was collected. The concentration of metal ions in supernatant was measured using flame atomic absorption spectrophotometer (AAS). The effect of time on the adsorption of Cr (VI) ions on adsorbent was studies in a range of 5–300 min. The amount of metal ions adsorbed onto adsorbent was calculated by a mass balance relationship:

$$q_e = \frac{(C_o - C_e)V}{W} \quad (1)$$

where, q_e is the amount of metal ion adsorbed per unit weight of the adsorbent (mg g^{-1}); C_o and C_e are the concentrations (mg L^{-1}) of the metal ion before and after adsorption, respectively; V is the volume of the adsorption medium (L); W is the amount of the adsorbent (g).

3. Results and discussion

3.1. Adsorbent characterization

The FT-IR spectra of MMT, CTAB-MMT, chitosan, PANI and CPOM are shown in Fig. 1 in which Na–MMT showed the peak at 1,046 cm^{-1} due to Si–O stretching, the peak at 3,640 cm^{-1} due to the stretching mode of –OH bond [24]. The peak at 1,636 cm^{-1} is also associated with the RN $(CH_3)^{3+}$ ion in CTAB. Besides, the peaks at 2,851–3,018 cm^{-1} are due to the stretching of $–CH_2$ group, which comes from CTAB with long

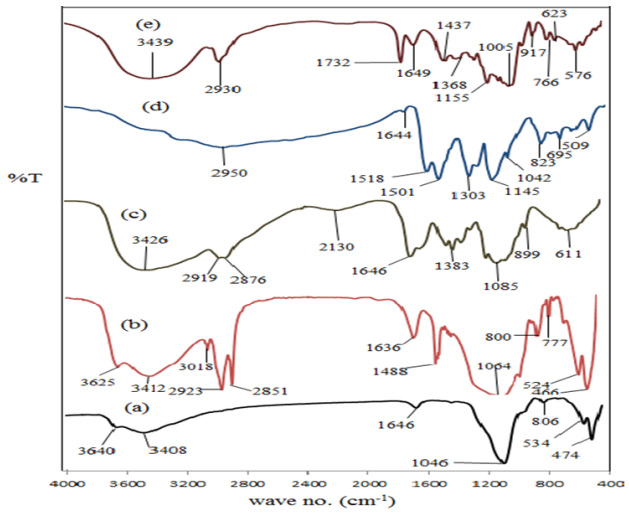

Fig. 1. FT-IR spectrum of (a) MMT, (b) CTAB-MMT, (c) Chitosan (d) PANI, (e) CPOM.

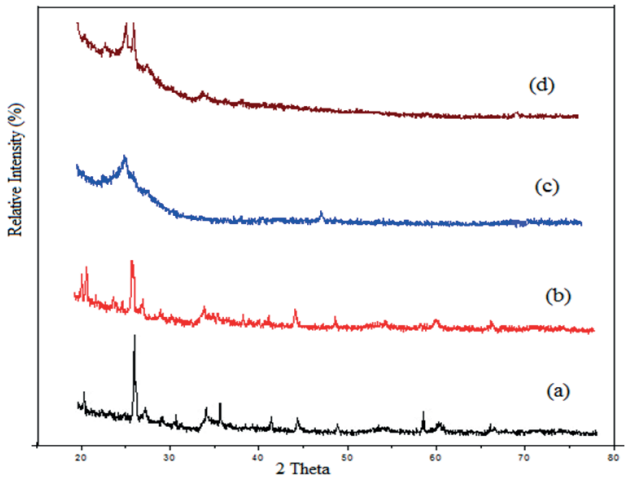

Fig. 2. XRD spectra of (a) MMT, (b) CTAB-MMT, (c) PANI, (d) CPOM.

aliphatic tail in their molecules [25]. The presence of broad peak at 3,426 cm^{-1} in the spectrum of chitosan is of hydroxyl groups while peaks appearing at 1,646 cm^{-1} and 1,383 cm^{-1} correspond to stretching vibrational frequency of amide I and amide II in chitosan molecules [26]. In the spectra of PANI, the peaks from 1,501 to 1,644 cm^{-1} are attributed to the characteristic C–C stretching of the quinoid and benzenoid rings. Finally the spectra of CPOM nanocomposite, the broad peak at 3,439 cm^{-1} is due to overlapping of –OH bands from CTS, MMT and –NH2 peaks from PANI. The Ar-H band of PANI is overlapped with –OH bands of CTS and MMT.

XRD patterns of MMT, OMMT, PANI and CPOM are shown in Fig. 2. The diffraction peak of the OMMT occurring at 2θ = 28.94°, corresponding to 3.336A° shifted from that of Na-MMT (2θ = 26.69°), corresponding to 3.01A°. These indicated that the cation exchange is intercalated into the galleries of silicate layers after exchanging with the sodium ion. The PANI peak diffracted at an angle of 2θ = 25.72°,

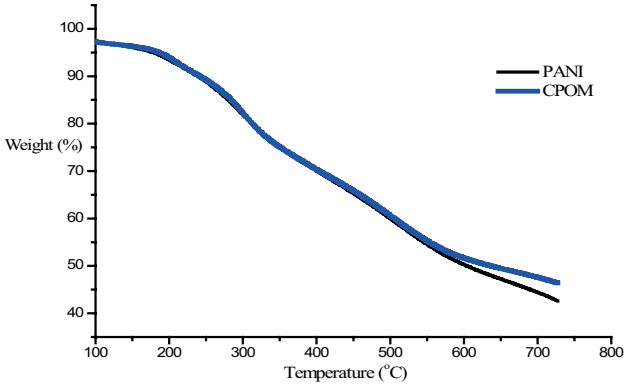

Fig. 3. TGA thermograms of PANI and CPOM.

respectively, in the XRD pattern showing low crystallinity for conductive polymers due to the repetition of benzenoid and quinoid rings in PANI chains [27]. The XRD pattern of nanocomposite material contains all the peaks related to OMMT and PANI with reduced intensity demonstrating a complete incorporation OMMT in CTS-PANI matrix. The Strong peak in XRD spectra of PANI vanishes in the CPOM spectra due to grafting with chitosan.

Thermal stability of PANI and its composite was analysed by TGA and the thermograms are given in Fig. 3. The TGA thermogram of pure PANI shows three step degradation of weight in the range of 30°C–800°C. The first weight loss of at around 120°C is due to evaporation of water. The second stage of weight loss starting at around 140°C up to 370°C almost 60% substance weight loss which represents the degradation of low molecular weight polymers [28]. From 370°C onwards, degradation of PANI Chains takes place up to 800°C in which almost 90% mass loss is observed. The CPOM also shows same stages of weight loss with little bit of higher thermal stability as compared with pure PANI due to incorporation of OMMT in CTS-PANI matrix.

The surface morphology of CPOM was studied by scanning electron microscopy taken PANI and chitosan as reference. As can be seen in Fig. 4, chitosan showed cotton like accumulation and carrying an irregular shape with smooth surface while close packed particles with amorphous nature is observed in the SEM image of PANI. The SEM image of CPOM nanocomposite reveals a close mapping of spherical particles with porous surface showing an enhanced crystalline morphology of nanocomposite.

Typical TEM image of CPOM nanocomposite is shown in Fig. 5, which indicates the presence of relatively spherical structures and well disperse distribution of the OMMT nanoclay in the CTS-PANI matrix. According to Fig. 5, the average size of OMMT nanoclay was estimated to be 93.42 nm.

3.2. Adsorption behaviour of CPOM for Cr (VI) and Cd (II)

3.2.1. Effect of contact time and adsorbent dose

To evaluate the effect of contact time for removal of Cr (VI) and Cd (II), 20 mL of 40 mg L^{-1} metal ion solution was taken in time intervals of 5 to 300 min. From Fig. 6 (a), it can be observed that the equilibrium was achieved within 120 min after which it became constant and there was no further

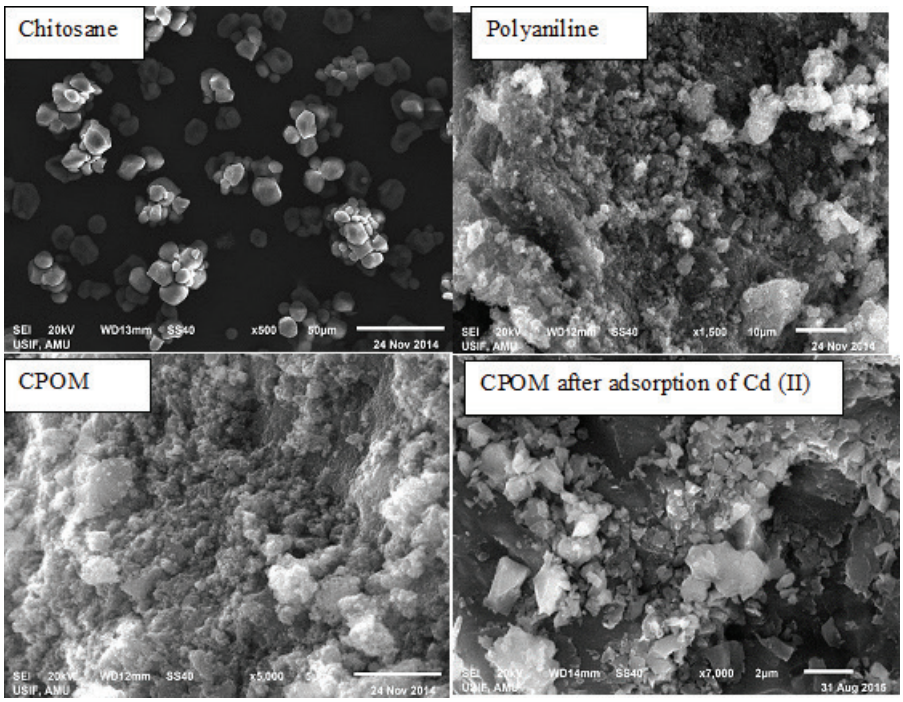

Fig. 4. SEM images of chitosan, PANI and CPOM before and after adsorption.

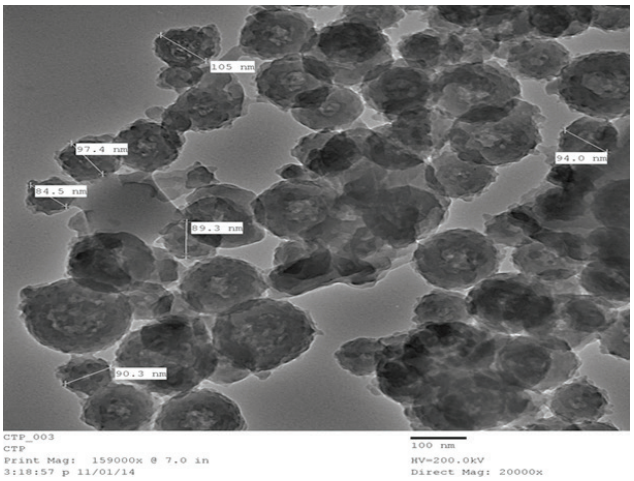

Fig. 5. TEM image of CPOM showing particle size and its distribution in polymer matrix.

metal ion adsorption was observed. Hence, 120 min contact time was chosen as optimum time for further experiments so that complete equilibrium is achieved within this time period. The process was found to be very rapid initially, and a large fraction of the metal ions were removed within few minutes attributing to the availability of a large number of vacant sites are available for adsorption initially. After some time, the remaining vacant sites are not easily available due to repulsive forces between the metal ions on the solid surface and the bulk phase resulting in slowing the removal process.

The adsorption of metal ions in the solution is greatly affected by the dose of adsorbent used. A range of adsorbent dose from 10 to 100 mg was used with 20 mL of 50 mg L^{-1} of metal ion solution for 120 min to investigate the effect of dose on removal of metal ions and the results are shown in Fig. 6 (b). It was found that the adsorption efficiency for both metal ion increases as the amount of adsorbent increase but for Cr (VI) removal efficiency decreases after 70 mg while for Cd (II) removal efficiency slightly increases with increase in adsorbent dose. This trend can be explained as the adsorbent dose increases, the number of adsorbent particles also increases facilitating more active sites for adsorption.

3.2.2. *Effect of pH*

In order to evaluate the influence of pH on the adsorption capacity of the CPOM, experiments were carried out at initial metal ion concentration of 40 mg L^{-1} and in the pH range 1.0–7.0. It can be seen from Fig. 6 (c) that an abrupt increase in adsorption capacities for Cr (VI) was observed when pH increases up to 2 while for Cd (II) up to 5 and then decrease slightly with further increase of pH values. At pH<4, due to presence of excess of H+ ions in the solution the adsorbent surface becomes positively charged due to protonation and $HCrO_4^-$ form of Cr (VI) ions are dominant at lower pH [29], so strong electrostatic attraction between positively charged adsorbent surface and negatively charged $HCrO_4^-$ ions leads to higher removal efficiency. However, as the pH increases deprotonation of surface of the adsorbent was occurred due to decrease in no. of H^+ ions as a result lower adsorption capacity obtained due to less interaction between Cr (VI) ions and adsorbent surface at higher pH value. At pH > 5.0, precipitation of metal as metal oxide occurs leading to decrease in adsorption efficiency and at pH < 5.0, H^+ ions in the solution competes with the metal ion for adsorption resulting in poor adsorption capacity for Cd (II) [30]. Therefore, pH 5.0 is

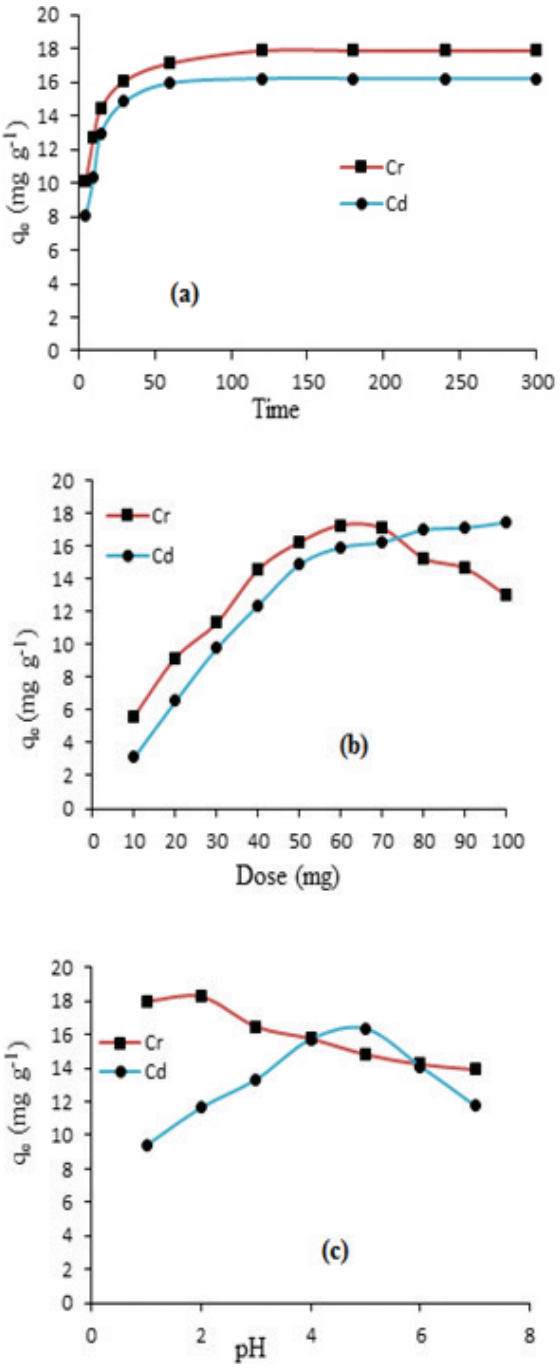

Fig. 6. Effects of (a) contact time, (b) dose, (c) pH on adsorption of Cr (VI) and Cd (II) on CPOM at 50°C with C_o = 40 mg L^{-1}.

considered as optimum pH for Cd (II) as maximum adsorption capacity was obtained at this pH.

3.3. Adsorption isotherm modeling

An important aspect that must be considered in adsorption reactions for the removal of heavy metal ions from aqueous solutions is the fitting of the experimental data obtained to a corresponding adsorption isotherm model. The experimental data were applied to three adsorption isotherm model such as Langmuir, Freundlich and Flory-Huggins and Temkin [31–34]. The parameters for all the models are calculated by linear regression method and listed in Table 1.

Linear form of equations for Langmuir, Freundlich, Flory-Huggins, and Temkin model is given as follows:

$$\frac{C_e}{q_e} = \frac{1}{q_m K_L} + \frac{C_e}{q_m} \tag{2}$$

$$\ln q_e = \frac{1}{n}\ln C_e + \ln K_F \tag{3}$$

$$\ln\left(\frac{\theta}{C_e}\right) = \ln K_{FH} + n\ln(1-\theta) \tag{4}$$

$$q_e = B\ln A + B\ln C_e \tag{5}$$

$$B = \frac{RT}{b} \tag{6}$$

where C_e is the equilibrium concentration of metal ions (mg L^1), q_e is the adsorption amount at the equilibrium (mg g^{-1}), q_m is the maximum adsorption capacity (mg g^{-1}), and K_L is the Langmuir constant related to the affinity of binding sites (L mg^{-1}). The value of q_m and K_L can be calculated by slope and intercept of a plot between C_e/q_e and C_e (Fig. 7(a)).

K_F is roughly an indicator of the adsorption capacity and n is the adsorption intensity which is a numerical value and varies with heterogeneity. The magnitude of the exponent n gives an indication of the favourability of adsorption. For a favourable adsorption, value of n must be greater

Table 1
Adsorption isotherm parameters for Cr (VI) and Cd (II) on CPOM at 50°C

Ions	Langmuir			Freundlich			Flory-Huggins				Temkin		
	q_m	K_L	R^2	n	K_F	R^2	n	K_{FH}	ΔG	R^2	A	b	R^2
Cr (VI)	90.90	0.06	0.99	1.27	44.51	0.98	0.23	18.99	–7.91	0.96	2.19	220.66	0.98
Cd (II)	54.64	0.02	0.99	1.09	5.08	0.98	0.26	7.72	–7.72	0.98	1.38	231.90	0.98

Note: q_m (mg g^{-1}), K_L (L mg^{-1}), K_F [mg g^{-1}(L/mg)$^{1/n}$], b (L mg^{-1}), A (L g^{-1}), ΔG (KJ mol^{-1}), A (L mg^{-1}), b (J mol^{-1}), K_{FH} (L g^{-1}).

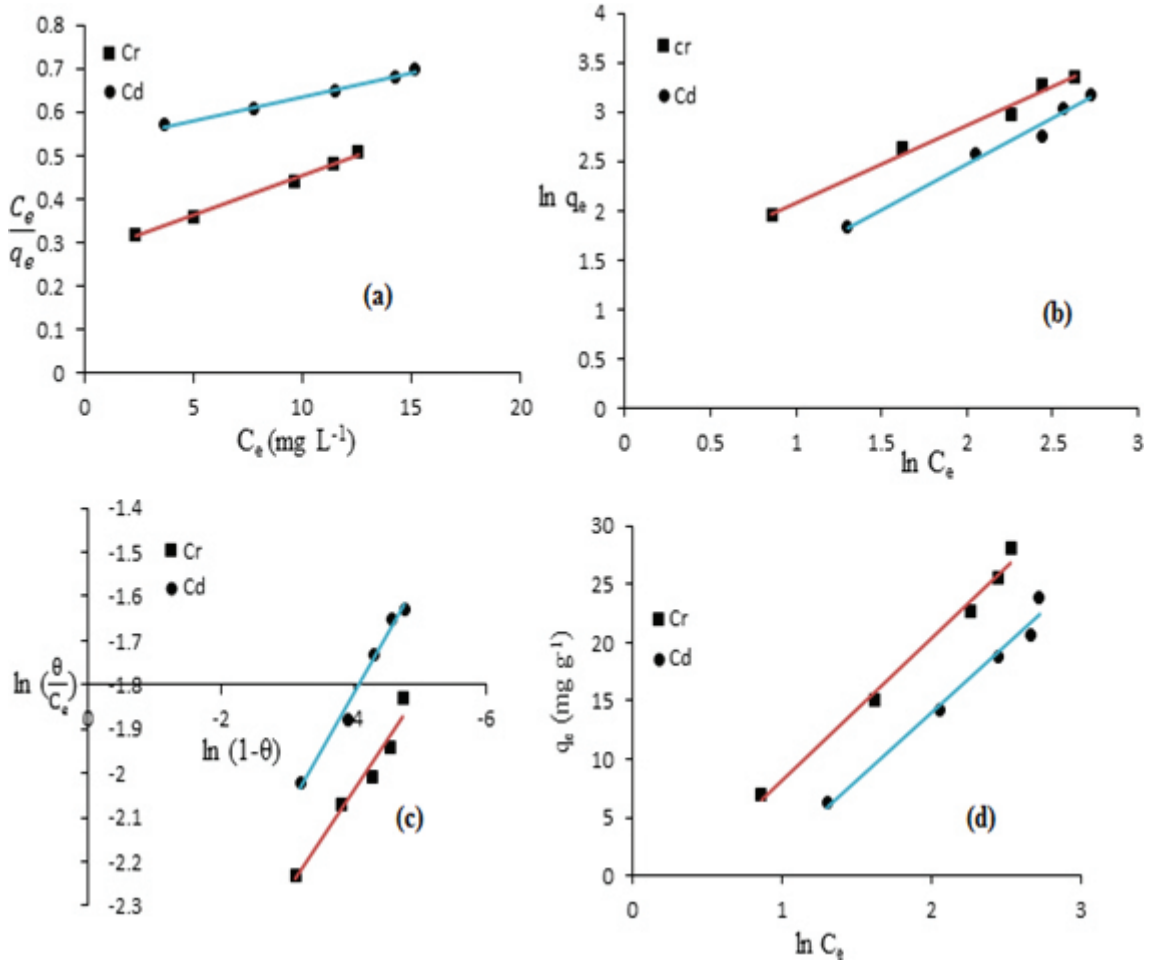

Fig. 7. (a) Langmuir, (b) Freundlich, (c) Flory-Huggins, (d) Temkin - adsorption isotherms for Cr (VI) and Cd (II) on CPOM at 50°C, 0.05 g of adsorbent & optimum pH.

than unity. K_F and n can be calculated by a linear plot between ln q_e and ln C_e (Fig. 7(b)).

θ = (1–C_e/C_o) is the degree of surface coverage, n is the number of adsorbate occupying adsorption sites, K_{FH} is the equilibrium constant (L mol^{-1}). K_{FH} and n can be determined by plotting ln (θ/C_o) vs. ln (1–θ) (Fig. 7(c)) and the parameters are given in Table 1. K_{FH} and ΔG° are related as follows;

$$\Delta G^{o} = -RT \ln K_{FH} \quad (7)$$

where ΔG° is the standard free energy change, R is the universal gas constant and equal to 8.314 J mol^{-1} K^{-1} and T is the absolute temperature. The values of ΔG° calculated was negative which shows that the adsorption process is spontaneous in nature.

Temkin isotherm model assumes that the heat of adsorption of all the metal ions in the layer decreases linearly with the coverage of surface of adsorbent and the ongoing process of adsorption can be characterized by uniform distribution of binding energies up to maximum value of binding energy for that process. Thus, a plot of ln C_e as function of amount of metal ion adsorbed at equilibrium give straight lines indicating thereby uniform distribution of binding energy is taking place because of interaction of the adsorbing metal ions. The slope and intercept of straight line evaluates A the binding constant corresponding to binding energy in L mg^{-1} and B the heat of adsorption in J mol^{-1} that can be calculated from the slope and intercept of the plot between q_e and ln C_e given in Fig. 7 (d).

The adsorption parameters calculated by linear plots are given in Table 1. The value of linear regression coefficient (R^2) obtained for Freundlich for both Cr (VI) and Cd (II) is 0.99 that is higher than the Langmuir, Flory-Huggins and Temkin, demonstrating that the equilibrium data were best fitted with Freundlich adsorption model. The maximum monolayer adsorption capacity obtained by Langmuir 90.90 mg g^{-1} for Cr (VI) and 54.64 mg g^{-1} for Cd (II) suggesting that the material has more affinity for Cr (VI) than the Cd (II). The value of n obtained from Freundlich isotherm model also greater than unity indicating that the adsorption is favourable for both the metal ions. The free energy values calculated by Flory-Huggins support the spontaneous nature of adsorption process and they are in close relation to the values obtained by thermodynamic studies at 50°C. On observing the values of binding constant A from Table 1,

they also support for the high affinity of Cr (VI) towards adsorbent as compare with Cd (II).

3.4. Adsorption kinetics

For a practical application of CPOM in heavy metal removal, kinetics of the adsorption reaction is required. A number of kinetic models have been established to understand the adsorption kinetics and rate-limiting step such as pseudo-first-order [35], pseudo-second-order [36] and Weber-Morris intraparticle diffusion [37]. The linear equations for these models are given as follows;

The linear equations for pseudo-first-order, pseudo-second-order and intraparticle diffusion model are given as:

$$\log(q_e - q_t) = \log q_e - \frac{k_1}{2.303}t \tag{8}$$

$$\frac{t}{q_t} = \frac{1}{k_2 qe^2} + \frac{t}{q_e} \tag{9}$$

$$q_t = \frac{1}{\beta}\ln t + \frac{1}{\beta}\ln(\alpha\beta) \tag{10}$$

$$q_t = k_{int}t^{1/2} + C \tag{11}$$

where q_e (mg g^{-1}) is the equilibrium adsorption capacity, q_t (mg g^{-1}) is the adsorption capacity at time t and k_1 (min^{-1}) is the pseudo-first-order rate constant and k_2 is the pseudo-second-order rate constant (g mg^{-1} min^{-1}). Values of k_1 and q_e can be obtained from the slope and intercept of the plot of log (q_e–q_t) and t given in Fig. 8 (a–d). α is the initial adsorption rate (mg g^{-1} min^{-1}) and β is the adsorption constant (g mg^{-1}). The plot of q_t vs. $t^{1/2}$ at different initial solution concentrations gives the value of k_{int} and may present multi linearity which indicates two or more steps occurring in the adsorption process.

The calculated data for both the models are listed in Table 2 from which it can be interpreted that the correlation factor obtained for pseudo-second-order model (0.99) is higher than the pseudo-first-order (0.98), Elovich (0.88) and intraparticle (0.63), indicating thereby involvement of pseudo-second-order process for both the metal ions. Furthermore, the calculated

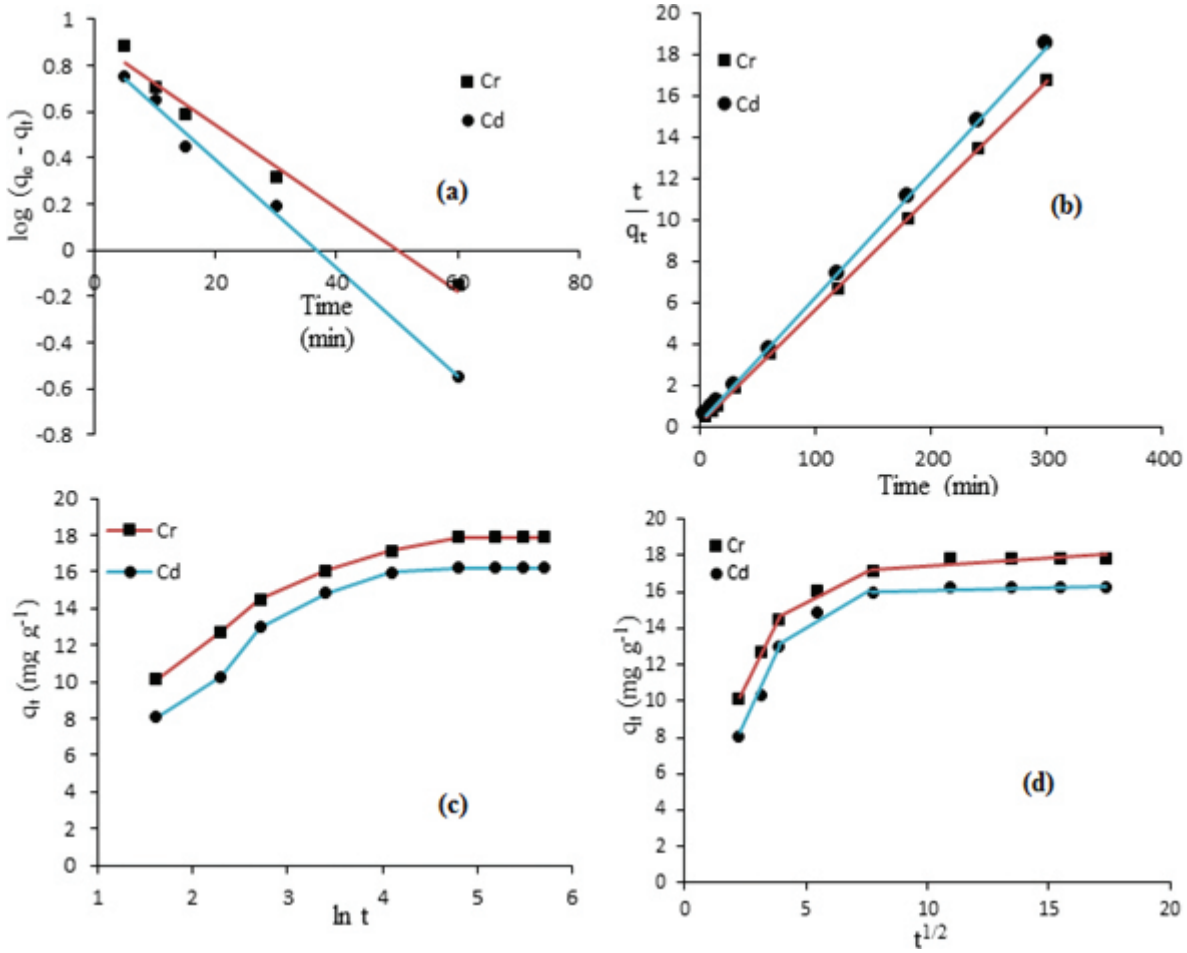

Fig. 8. (a) Pseudo-first-order, (b) Pseudo-second-order, (c) Elovich, (d) Intraparticle diffusion model for Cr (VI) and Cd (II) on CPOM at 50°C taking 0.05 g of adsorbent at optimum pH and 40 mg L^{-1} as initial metal ion concentration.

Table 2
Kinetic parameters for Cr (VI) and Cd (II) ions at 50°C

Metal ions	Pseudo-first-order			Pseudo-second-order			Elovich			Intra-particle		
	$q_e$cal	k_1	R^2	$q_e$cal	k_2	R^2	α	β	R^2	K_{int}	C	R^2
Cr (VI) (q_{exp} = 17.88)	8.06	0.042	0.984	18.15	0.015	0.99	295.96	0.58	0.88	0.41	12.14	0.68
Cd (II) (q_{exp} = 16.23)	7.23	0.054	0.99	16.52	0.015	0.99	72.75	0.54	0.84	0.43	10.33	0.63

values of q_e by using pseudo-second-order rate equation and the experimental values were close to each other for both the metal ions as compared with pseudo-first-order rate equation, which shows a large deviation from the experimental values. This phenomenon further indicates that the adsorption kinetics for the uptake of heavy metals on CPOM nanocomposite can be best described by pseudo-second-order rate equation and chemical sorption involving valences forces through sharing or exchanging of electrons between sorbate and sorbent may be the rate controlling process.

3.5. Thermodynamics of adsorption

To confirm our prediction about the endothermic nature of the adsorption process, thermodynamic parameters such as Gibbs free energy change (ΔG°), enthalpy change (ΔH°) and entropy change (ΔS°) were calculated using the Gibbs equation and the van't Hoff equation given below:

$$\Delta G^o = -RT \ln K_c \tag{12}$$

$$\ln K_c = -\frac{\Delta H^o}{R} + \frac{\Delta S^o}{RT} \tag{13}$$

The gas constant R is defined by 8.3145 J mol^{-1} K^{-1}. K_c (C_{ad}/C_e) is the distribution coefficient; T is the temperature of the solution in Kelvin. ΔG° and ΔS° were calculated from the slope and intercept of a plot of ln K_c as a function of 1/T, as shown in Fig. 9. The free energy change (ΔG°) can be determined from the following equation.

$$\Delta G^o = \Delta H^o - T\Delta S^o \tag{14}$$

Thermodynamic parameters associated with the Cr (VI) and Cd (II) adsorption by the nanocomposite are listed in Table 3. The positive value of ΔH° confirmed the endothermic nature of the adsorption process of the nanocomposite for the adsorption of Cr (VI) and Cd (II). The values of ΔG° are all negative, and the value of ΔG° decreases as the temperature increase from 30°C–50°C, which indicates that the Cr (VI) and Cd (II) adsorption process of the nanocomposite is spontaneous and spontaneity increases with temperature [38]. The positive value of ΔS° reveals the increased randomness at the solid-solution interface during the binding of the metal ions on the active sites of the CPOM nanocomposite.

3.6. Comparison with other adsorbents

A comparison of adsorption capacities of various adsorbents with the present study has been given in Table 4. The table itself reveals that the present adsorbent shows a high adsorption capacity towards Cr (VI) and Cd (II). The comparison of metal ions adsorption on nanocomposite and other individual components have been presented in Fig. 10 that clearly indicates that CPOM nanocomposite exhibit highest adsorption efficiency towards both metal ions.

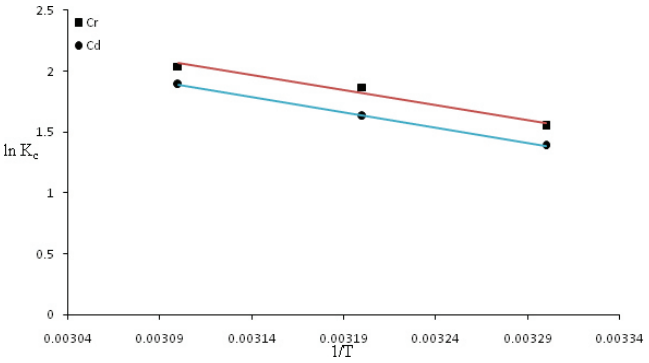

Fig. 9. Thermodynamic plot between ln Kc and 1/T for removal of Cr (VI) and Cd (II) on CPOM at 30, 40 and 50°C.

Table 3
Thermodynamic parameters for Cr (VI) and Cd (II) onto CPOM as a function of temperature

Metal ions	ΔH° KJ mol^{-1}	ΔS° KJ K^{-1} mol^{-1}	ΔG° (KJ mol^{-1}) 303K	313K	323K
Cr (VI)	20.37	0.080	–3.88	–4.69	–5.49
Cd (II)	20.79	0.088	–3.49	–4.29	–5.09

Table 4
Comparison of adsorption capacities (mg g^{-1}) of various adsorbents

Adsorbent	Cr (VI)	Cd (II)	References
Ce (III) doped $ZnFe_2O_4$	57.24	–	[39]
Fly Ash/chitosan	–	87.72	[40]
Halomonas BVR1/chitosan	–	23.88	[41]
HCB/TiO_2	27.33	–	[42]
SSMS	47.61	–	[43]
MnO_2/o-MWCNTs	–	41.60	[44]
Imidazole/silica	47.79	–	[45]
PGC	–	14.33	[46]
CPOM	123.45	84.75	This Study

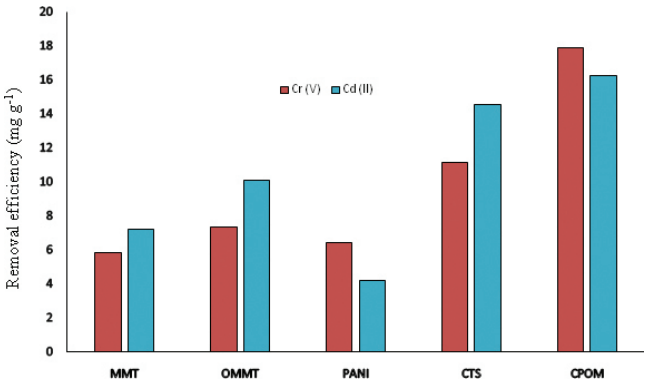

Fig. 10. Comparison of removal efficiency of individuals with CPOM for Cr (VI) and Cd (II).

4. Conclusion

In the present study, chitosan-g-polyaniline/OMMT (CPOM) was synthesized by oxidative free radical polymerization of aniline in presence of chitosan and OMMT. The material was well characterized by FT-IR, XRD, TGA, SEM and TEM and further used for the removal of Cr (VI) and Cd (II). Batch experiments were performed to study the effects of contact time, solution pH and adsorbent dose. The results showed that equilibrium was established after 120 min of contact. The adsorption of metal ions is highly pH-dependent and the maximum removal efficiencies and adsorption capacities of the selected metal ions were obtained at pH values 2 for Cr (VI) and 5 for Cd (II). The equilibrium data were applied to four isotherm model Langmuir, Freundlich and Flory-Huggins and Temkin model and best fitted with Freundlich isotherm model and maximum monolayer adsorption capacity calculated by Langmuir model was found to be 90.90 mg g^{-1} for Cr (VI) and 54.64 mg g^{-1} for Cd (II) at 50°C. All kinetic results suggest that the adsorption of metal ions by CPOM followed the second order kinetics model and chemisorption is the rate determining step. Thermodynamic studies reveals that the adsorption process for removal of Cr (VI) and Cd (II) is spontaneous and feasible based the calculated free energy values.

Acknowledgements

The authors gratefully acknowledge the instrumentation laboratory, Centre for Excellence in Nanomaterials Department of Applied Physics AMU, Sophisticated Analytical instrumentation facility (SAIF) Punjab University Chandigarh, University Sophisticated Instrumentation facility (AMU), STIC Cochin and are highly thankful to UGC-MANF New Delhi for providing financial assistance.

References

[1] M.Q. Jiang, X.Y. Jin, X.Q. Lu, Z.L. Chen, Adsorption of Pb(II), CdI(II), Ni(II) and Cu(II) onto natural kaolinite clay, Desalination, 252 (2010) 33–39.
[2] T. S. Anirudhan, S. S. Sreekumari, Adsorptive removal of heavy metal ions from industrial effluents using activated carbon derived from waste coconut buttons, J. Environ. Sci., 23 (2011) 1989–1998.
[3] Y. Wang, B. Zou, T. Gao, X. Wu, S. Lou, S. Zhou, Synthesis of orange-like Fe3O4/PPy composite microspheres and their excellent Cr (VI) ion removal properties, J. Mater. Chem., 22 (2012) 9034–9040.
[4] Y. Wang, D. Liu, J. Lu, J. Huang, Enhanced adsorption of hexavalent chromium from aqueous solutions on facilely synthesized mesoporous iron–zirconium bimetal oxide, Coll. & Surf. A: Physicochem. Engg. Asp., 481 (2015) 133–142.
[5] A. Mittal, Mu. Naushad, G. Sharma, Z. A. ALothman, S.M. Wabaidur, M. Alam, Fabrication of MWCNTs/ThO_2 nanocomposite and its adsorption behavior for the removal of Pb (II) metal from aqueous medium, Desal. Water Treat., (2015) doi: 10.1080/19443994.2015.1125805.
[6] N.R. Axtell, S.P.K. Sternberg, K. Claussen, Lead and nickel removal using Microspora and lemna minor, Bioresour. Technol., 89 (2003) 41–48.
[7] A. Bernard, Cadmium & its adverse effects on human health, Indian J. Med Res., 128 (2008) 557–564.
[8] Mu. Naushad, A. Mittal, M. Rathore, V. Gupta, Ion-exchange kinetic studies for Cd(II), Co(II), Cu(II), and Pb(II) metal ions over a composite cation exchanger, Desal. Water Treat., 54 (10) (2015) 2883–2890.
[9] K. Shin, J. Hong, J. Jang, Heavy metal ion adsorption behaviour in nitrogen-doped magnetic carbon nanoparticles: isotherms and kinetic study, J. Hazard. Mater., 190 (2011) 36–44.
[10] Z. A. AL Othman, M. Naushad, R. Ali, Kinetic, equilibrium isotherm and thermodynamic studies of Cr (VI) adsorption onto low-cost adsorbent developed from peanut shell activated with phosphoric acid, Environ. Sci. Poll. Res., 20 (2013) 3351–3365.
[11] Mu. Naushad, T. Ahamad, Z.A. Alothman, M.A. Shar, N.S. AlHokbany, S.M. Alshehri, Synthesis, characterization and application of curcumin formaldehyde resin for the removal of Cd^{2+} from wastewater: kinetics, isotherms and thermodynamic studies, J. Ind. Engg. Chem., 29 (2015) 78–86.
[12] M.A. Tofighy, T. Mohammadi, Adsorption of divalent heavy metal ions from water using carbon nanotube sheets, J. Hazard. Mater., 185 (2011) 140–147.
[13] M. Naushad , Z.A. AL Othman, M.R. Awual, M.M. Alam, G.E. Eldesoky, Adsorption kinetics, isotherms, and thermodynamic studies for the adsorption of Pb2+ and Hg2+ metal ions from aqueous medium using Ti (IV) iodovanadate cation exchanger, Ionics, 21 (2015) 2237–2245.
[14] W.S. Wan Ngah, L.C. Teong, M.A.K.M. Hanafiah, Adsorption of dyes and heavy metal ions by chitosan composites: a review, Chem. Mater., 15 (2003) 1446–1456.
[15] E. Igberase, P. Osifo Equilibrium, kinetic, thermodynamic and desorption studies of cadmium and lead by polyaniline grafted cross-linked chitosan beads from aqueous solution, J. Indus. & Engg. Chem., 26 (2015) 340–347.
[16] M. Rinaudo, Chitin and chitosan: properties and application, Prog. Polym. Sci., 31 (2006) 603–632.
[17] R. Ahmad, R. Kumar, Conducting polyaniline/iron oxide composite: a novel adsorbent for the removal of amido black 10B, J. Chem. Eng. Data, 55 (2010) 3489–3493.
[18] F. Kanwal, R. Rehman, J. Anwar, M. Saeed, Batchwise removal of chromium (VI) by adsorption on novel synthesized polyaniline composites with various brans and isothermal modelling of equilibrium data, J. Chem. Soc. Pak., 34 (2012) 1134–1139.
[19] J. Zhu, H. He, L. Zhu, X. Wen, F. Deng, Characterization of organic phases in them interlayer of montmorillonite using FTIR and 13C NMR, J. Colloid Interface Sci., 286 (2005) 239–244.
[20] L. Janovak, J. Varga, L. Kemeny, I. Dekany, Swelling properties of copolymer hydrogels in the presence of montmorillonite and alkylammonium montmorillonite, Appl. Clay Sci., 43 (2009) 260–270.
[21] Y. Tang, Y. Hu, L. Song, Z. Gui, Z. Chen, W. Fan, Preparation and thermal stability of polypropylene/montmorillonite nanocomposites, Polym. Degrad. Stab., 82 (2003) 127–131.
[22] S.G. Abd Alla , R.H. Helal, A.W.M. El-Naggar, Characterization of poly(vinyl alcohol)/acrylamide/alkylammonium montmorillonite clay nanocomposites prepared by electron beam irradiation, Adv. Compos. Mater., 24 (2015).

[23] S. Sedaghat, Synthesis and characterization of new biocompatible copolymer: chitosan-graft polyaniline, Interna. Nano Letters, 4 (2014).
[24] G.V. Joshi, B.D. Kevadiya, H.A. Patel, H.C. Bajaj, R.V. Jasra, Montmorillonite as a drug delivery system: Intercalation and in vitro release of timolol maleate, Int. J. Pharm., 374 (2009) 53–57.
[25] W. Hoidy, M. Ahmad, A. Mulla, N.A. Ibrahim, Synthesis and characterization of organoclay from sodium montmorillonite and fatty hydroxamic acid, Am. J. Appl. Sci., 6 (2009) 1567–1572.
[26] L. Shi, X. Wang, L. Lu, X. Yang, X. Wu, Preparation of TiO2/polyaniline nanocomposite from a lyotropic liquid crystalline solution, Synth. Met., 159 (2009) 2525–2529.
[27] A.L. Sharma, V. Saxena, S. Annopoorni, B.D. Malhotra, Synthesis and characterization of a copolymer: Poly (aniline-co-fluoroaniline), J. Appl. Polym. Sci., 81 (2001) 1460–1466.
[28] X. Wang, A. Wang, Removal of Cd (II) from aqueous solution by a composite hydrogel based on attapulgite, Environ. Techn., 31 (2010) 745–753.
[29] A.G. Yavuz, E. Dincturk-Atalay, A. Uygun, F. Gode, E. Aslan, A comparison study of adsorption of Cr (VI) from aqueous solutions onto alkyl-substituted polyaniline/chitosan composites, Desalination, 279 (2011) 325–331.
[30] E.A. Ali, S.S. Elkholy, R.E. Morsi, M.Z. Elsabee, Studies on adsorption behavior of Cu (II) and Cd (II) onto aminothiophene derivatives of Styrene Maleic anhydride copolymer, J. Taiwan Inst. Chem. Engg., 64 (2016) 325–335.
[31] I. Langmuir, Adsorption of gaseous on plane surface of glass, mica and platinum, J. Am. Chem. Soc, 40 (1918) 1361–1403.
[32] H.M.F. Freundlich, Over the adsorption in solution, Z. Phys. Chem., 57 (1906) 385–470.
[33] A. Ergene, K. Ada, S. Tan, H. Katircioglu, Removal of Remazol Brilliant Blue R dye from aqueous solutions by adsorption onto immobilized Scenedesmus quadricauda: equilibrium and kinetic modeling studies, Desalination, 249 (2009) 1308–1314.
[34] M.J. Temkin, V. Pyzhev, Kinetics of ammonia synthesis on promoted iron catalysts, Acta Physiochim., 12 (1940) 217–222.
[35] S. Lagergren, About the theory of so-called adsorption of soluble substances, Handlingar, 24 (1898) 1–39.
[36] Y.S. Ho, Review of second-order models for adsorption systems, J Hazard. Mater., 136 (2006) 681–689.
[37] Jr. W.J. Weber, J.C. Morris, Kinetics of adsorption on carbon from solution, J. Sanit. Engg. Div: Am. Soc. Civil. Engg., 89 (1963) 31–59.
[38] B.H. Hameed, A.A. Ahmad, Batch adsorption of methylene blue from aqueous solution by garlic peel, an agricultural waste biomass, J. Hazard. Mater., 164 (2009) 870–875.
[39] S. Kuai, Z. Zhang, Z. Nan, Synthesis of Ce^{3+} doped $ZnFe_2O_4$ self-assembled clusters and adsorption of chromium (VI), J. Hazard. Mater., 250–251 (2013) 229–237.
[40] S. Pandey, S. Tiwari, Facile approach to synthesize chitosan based composite—characterization and cadmium (II) ion adsorption studies, Carbohyd. Polym., 134 (2015) 646–656.
[41] Manasi, V. Rajesh, N. Rajesh, An indigenous *Halomonas BVR1* strain immobilized in crosslinked chitosan for adsorption of lead and cadmium, Int. J Biolog. Macromol., 79 (2015) 300–308.
[42] L. Zhang, Y. Zhang, Adsorption characteristics of hexavalent chromium on HCB/TiO_2, App. Surf. Sci., 316 (2014) 649–656.
[43] S. Rangabhashiyam, N. Selvaraju, Efficacy of unmodified and chemically modified *Swietenia mahagoni* shells for the removal of hexavalent chromium from simulated wastewater, J. Mol. Liq., 209 (2015) 487–497.
[44] C. Luo, R. Wei, D. Guo, S. Zhang, S. Yan, Adsorption behavior of MnO_2 functionalized multi-walled carbon nanotubes for the removal of cadmium from aqueous solutions, Chem. Engg. J., 225 (2013) 406–415.
[45] Z. Wang, C. Ye, X. Wang, J. Li Adsorption and desorption characteristics of imidazole-modified silica for chromium (VI), App. Surf. Sci., 287 (2013) 232–241.
[46] R. Karthik, S. Meenakshi, Removal of Pb(II) and Cd(II) ions from aqueous solution using polyaniline grafted chitosan, Chem. Eng. J., 263 (2015) 168–177.